Particle swarm optimization for realizing bilayer thermal sensors with bulk isotropic materials

Peng Jin [a,*], Shuai Yang [a], Liujun Xu [a], Gaole Dai [b], Jiping Huang [a,*], Xiaoping Ouyang [c,*]

[a] Department of Physics, State Key Laboratory of Surface Physics, and Key Laboratory of Micro and Nano Photonic Structures (MOE), Fudan University, Shanghai 200438, China
[b] School of Sciences, Nantong University, Nantong 226019, China
[c] School of Materials Science and Engineering, Xiangtan University, Xiangtan 411105, China

ABSTRACT

Metamaterial-based devices have been extensively researched on account of their novel functions, such as cloaking, concentrating, rotating, and sensing. However, they are usually achieved by employing metamaterials with extreme parameters, critically restricting engineering preparation. To simplify parametric designs, we propose an optimization model with particle swarm algorithms to realize bilayer thermal sensors composed of bulk isotropic materials (circular structure). For this purpose, the fitness function is defined to evaluate the difference between the actual and expected temperatures. By choosing suitable materials for different regions and treating the radii of sensor, inner shell, and outer shell as design variables, we finally minimize the fitness function via particle swarm optimization. The designed scheme is not only easy to implement in applications, but shows excellent performances in both detective accuracy and thermal invisibility, which are well confirmed by finite-element simulations and laboratory experiments. Optimization model can also be flexibly extended to a square case. This method can not only calculate numerical solutions for difficult analytical theories (circular structure), but also calculate optimal solutions for problems without analytical theories (square structure), providing new inspiration for simplifying the design of metamaterials in a wide range of communities.

© 2021 Elsevier Ltd. All rights reserved.

1. Introduction

Novel meta-devices [1–24] have been researched continuously over the decades in various fields since the pioneering theoretical proposals of transformation theory [1–4]. Recently, many fruitful strategies have been proposed for offering new avenue of devising thermal meta-devices such as neutral inclusion [6], bilayer schemes [10], illusion thermotics [13], regionalization transformation [14], and many-particle thermal invisibility [21]. However, most experimental devices are prepared by employing metamaterials with unconventional thermal conductivities (i.e., anisotropic, graded or singular), which remain to be overcomed for engineering applications. New schemes deserve exploring for purpose of simplifying engineering preparation and developing novel functional meta-devices.

Optimization method has been conjectured as an effective tool for the design of metamaterials in the macro [25–33] or mi-

cro [34–36] scale, which is applied comprehensively in recent years. A gradient-based numerical optimization algorithm was used to control the heat flow in the printed circuit board [27]. Also, non-gradient-based black box algorithms including evolutionary algorithms have been used in the reverse structural design of thermal metamaterials [31]. On the basis of topology optimization [29,30,32,33], thermal meta-devices are reversely designed for specific objective functions, providing excellent performance. Whereas, topology optimization usually involves a change in structural topology, resulting in complex structural parameters. This inspires us to explore simpler structural meta-devices with equally high performance by employing optimization algorithms.

In this work, we propose an optimization model with particle swarm algorithms [37] (PSA) for designing bilayer thermal sensors composed of bulk isotropic materials. As an example, we design a circular bilayer thermal sensor with both detective accuracy and thermal invisibility. For this purpose, two objective functions are constructed simultaneously, one for detecting the temperature distribution of the region occupied by sensor with accuracy and the other for undisturbing the temperature distribution of original background. We treat the radius of sensor, inner shell and outer

* Corresponding authors.
   E-mail addresses: 19110190022@fudan.edu.cn (P. Jin), jphuang@fudan.edu.cn (J. Huang), oyxp2003@aliyun.com (X. Ouyang).

shell as design variables when choosing suitable material analogys for different regions. By adopting PSA, the characteristics of prescribed optimized structure are precisely and efficiently found. The designed scheme not only simplifies practical fabrication, but shows almost perfect performance, as both simulation result and experimental result exhibit. Optimization model can also be flexibly extended to a square case.

2. Theoretical analysis

The scheme for a bilayer thermal sensor is shown in Fig. 1(a). A sensor (with radii of R_1, Material 1) coated with a bilayer shell (inner shell with radii of R_2, Material 2; outer shell with radii of R_3, Material 3) is put in the center of background (Material 4) for detection of the temperature distribution of region occupied by it. Hot source and cold source are, respectively, set at the right-most and left-most boundaries. The up-most and down-most boundaries are thermally insulated. Temperature distributions follow Laplace equation with passive heat conduction at steady state:

$$\nabla \cdot \left(-\kappa(\boldsymbol{x}) \cdot \nabla T\right) = 0, \tag{1}$$

where $\kappa(\boldsymbol{x})$ is thermal conductivity, denoted by

$$\kappa(\boldsymbol{x}) = \begin{cases} \kappa_1 & \text{for } \boldsymbol{x} \text{ in region of Material 1,} \\ \kappa_2 & \text{for } \boldsymbol{x} \text{ in region of Material 2,} \\ \kappa_3 & \text{for } \boldsymbol{x} \text{ in region of Material 3,} \\ \kappa_4 & \text{for } \boldsymbol{x} \text{ in region of Material 4.} \end{cases} \tag{2}$$

Considering expanding Eq. (1) in cylindrical coordinates and symmetry of boundary conditions, the general solution of the temperature distribution in four regions can be expressed as:

$$T_1 = A_0 + Ar\cos\theta, \tag{3}$$

$$T_2 = A_0 + Br\cos\theta + Cr^{-1}\cos\theta, \tag{4}$$

$$T_3 = A_0 + Dr\cos\theta + Er^{-1}\cos\theta, \tag{5}$$

$$T_4 = A_0 + Fr\cos\theta + Gr^{-1}\cos\theta, \tag{6}$$

where A_0 is the temperature at $\theta = \pm\pi/2$, and $F = |\nabla T_0|$ represents the modulus of an external linear thermal field ∇T_0.

Boundary continuity conditions of temperature and normal heat flow should be satisfied,

$$\begin{cases} T_1(R_1) = T_2(R_1), \\ T_2(R_2) = T_3(R_2), \\ T_3(R_3) = T_4(R_3), \\ \left(-\kappa_1\dfrac{\partial T_1}{\partial r}\right)_{R_1} = \left(-\kappa_2\dfrac{\partial T_2}{\partial r}\right)_{R_1}, \\ \left(-\kappa_2\dfrac{\partial T_2}{\partial r}\right)_{R_2} = \left(-\kappa_3\dfrac{\partial T_3}{\partial r}\right)_{R_2}, \\ \left(-\kappa_3\dfrac{\partial T_3}{\partial r}\right)_{R_3} = \left(-\kappa_4\dfrac{\partial T_4}{\partial r}\right)_{R_3}. \end{cases} \tag{7}$$

When thermal sensor works, there is no thermal disturbances in sensor and background regions, which means we have following two equations:

$$\begin{cases} A = F, \\ G = 0. \end{cases} \tag{8}$$

So let's simplify the form of equations that are composed of Eqs. (7) and (8):

$$\begin{cases} FR_1 = BR_1 + CR_1^{-1}, \\ BR_2 + CR_2^{-1} = DR_2 + ER_2^{-1}, \\ DR_3 + ER_3^{-1} = FR_3, \\ -\kappa_1 F = -\kappa_2\left(B - CR_1^{-2}\right), \\ -\kappa_2\left(B - CR_2^{-2}\right) = -\kappa_3\left(D - ER_2^{-2}\right), \\ -\kappa_3\left(D - ER_3^{-2}\right) = -\kappa_4 F. \end{cases} \tag{9}$$

For given R_1, κ_1, κ_2, κ_3 and κ_4, we do have six unknown coefficients (B, C, D, E, R_2 and R_3) determined by six equations (Eq. (9)) uniquely. However, due to the nonlinear coupling of multiple unknowns, it is difficult to find an explicit analytical expression for
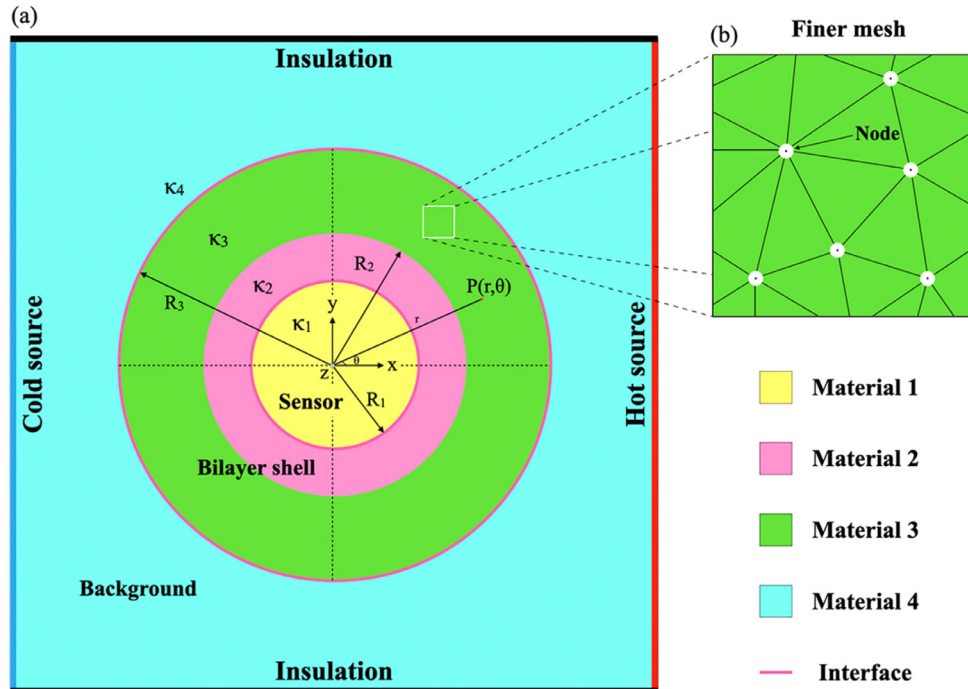

Fig. 1. (a) Schematic diagram for bilayer thermal sensors. (b) Discretized finer mesh for optimization.
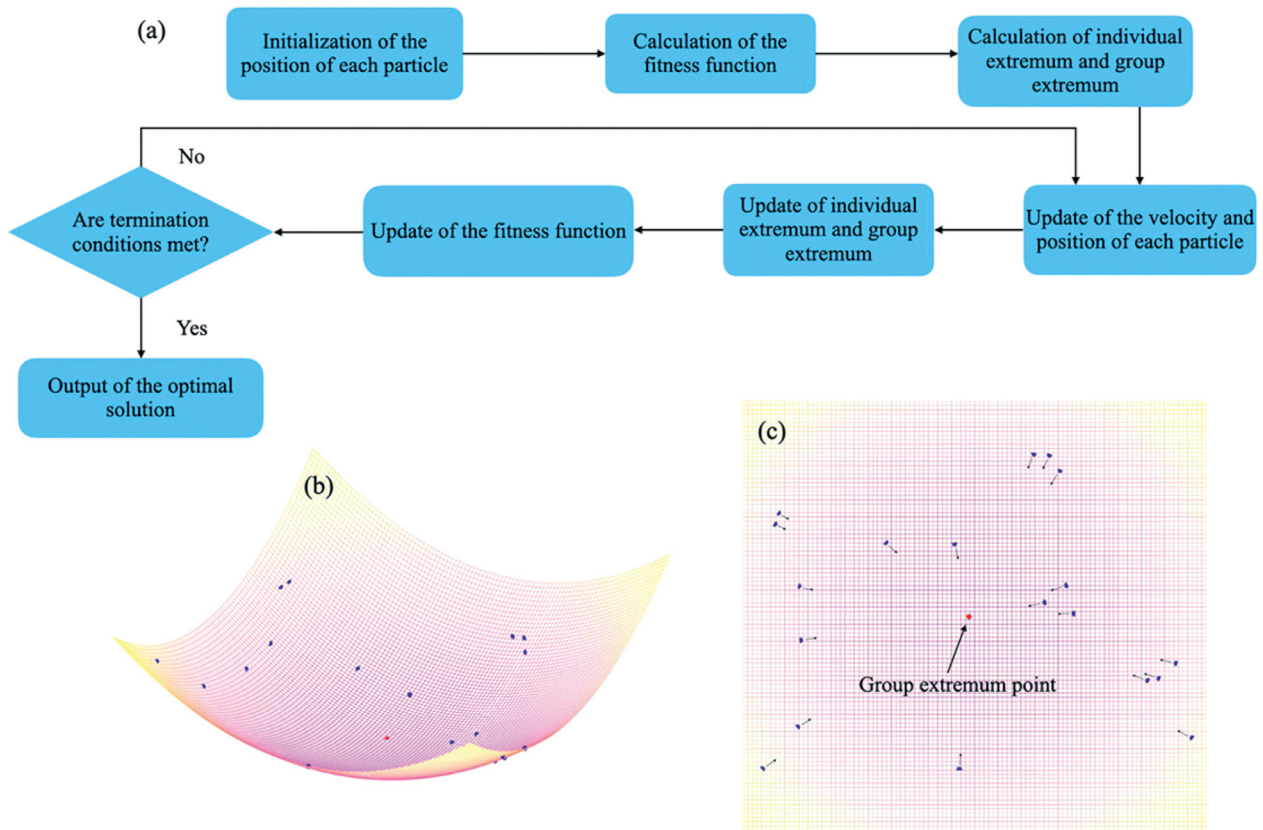
Fig. 2. (a) Illustration of the algorithm of PSA. (b) Schematic diagram of a particle swarm in search of an optimal solution. (c) Contour map of (b).
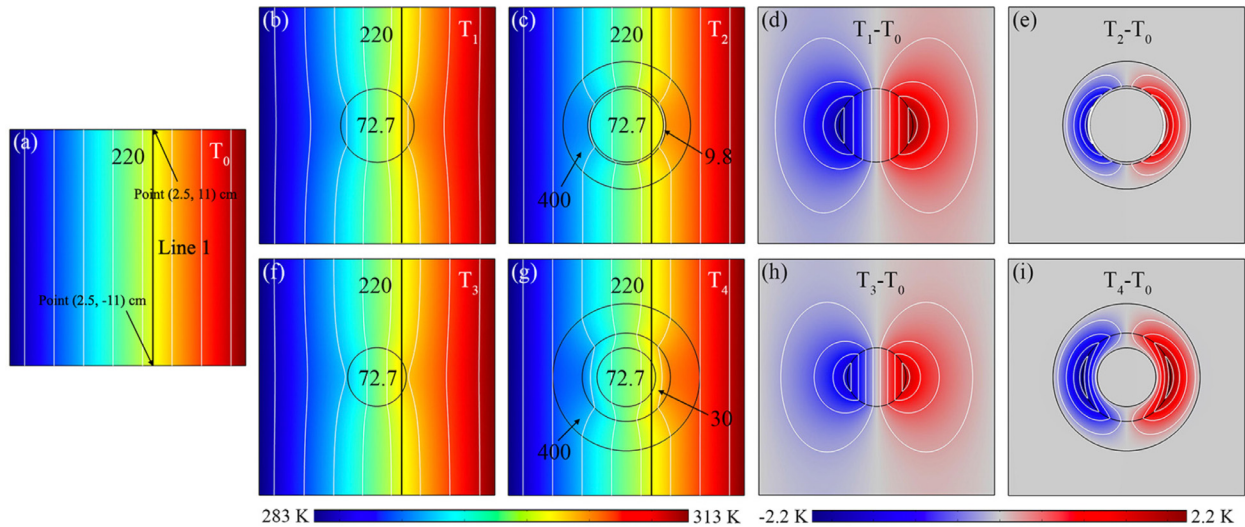

Fig. 3. Finite-element simulation results of circular bilayer thermal sensors. The simulation box is 22×22 cm^2. White lines represent isotherms. (a) Pure background for reference. (b),(c) First case for bare sensor with $R_1 = 3.42$ cm and bilayer thermal sensor with $R_1 = 3.42$ cm, $R_2 = 3.64$ cm, and $R_3 = 5.95$ cm. (f),(g) Second case for bare sensor with $R_1 = 2.73$ cm and bilayer thermal sensor with $R_1 = 2.73$ cm, $R_2 = 4.11$ cm, and $R_3 = 6.85$ cm. (d),(e) Temperature difference between (b),(c) and (a). (h),(i) Temperature difference between (f),(g) and (a).

any one radius. Only when the thermal conductivity of shell (circular or elliptic structure) is taken as unknown coefficients, can analytic expressions be obtained, which have great limitations. In this way, the physical image of the influence of geometric size on performance of thermal sensor cannot be given intuitively from the analytical theory. There is a mapping relationship between the radius of the circles (say, R_1, R_2 and R_3) and the performance of thermal sensor. We turn it into an optimization problem and reversely design the geometry size according to the performance.

3. Statement of optimization problem

In principle, a thermal sensor should have the ability of reproducing temperature distributions in sensor and background regions, which are the same as those in corresponding regions of original background [38]. The heat field to be studied is discretized for numerical optimization by using finer mesh in COMSOL MULTIPHYSICS [39], as shown in Fig. 1(b). Considering optimization problem, two objective functions for bilayer thermal sensors with accu-
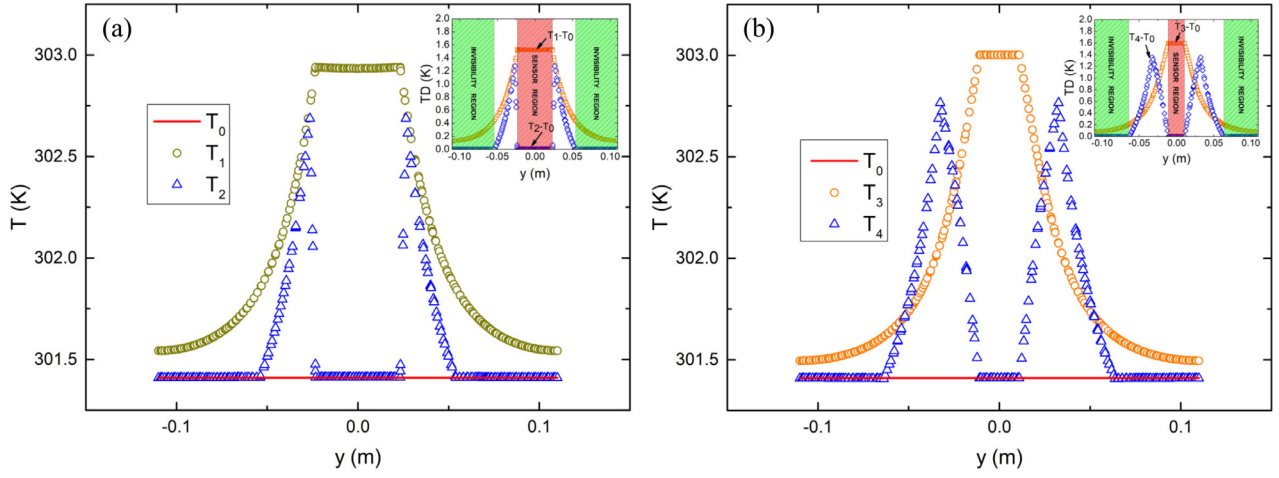
Fig. 4. Quantitative comparison of Fig. 3. (a) Temperature distributions (T_0, T_1, and T_2) on Line 1 in Fig. 3(a)–(c). Upper-right inset shows the temperature difference on Line 1 between T_1 (T_2) and T_0. (b) Temperature distributions (T_0, T_3, and T_4) on Line 1 in Fig. 3(a), (f), and (g). Upper-right inset shows the temperature difference on Line 1 between T_3 (T_4) and T_0.
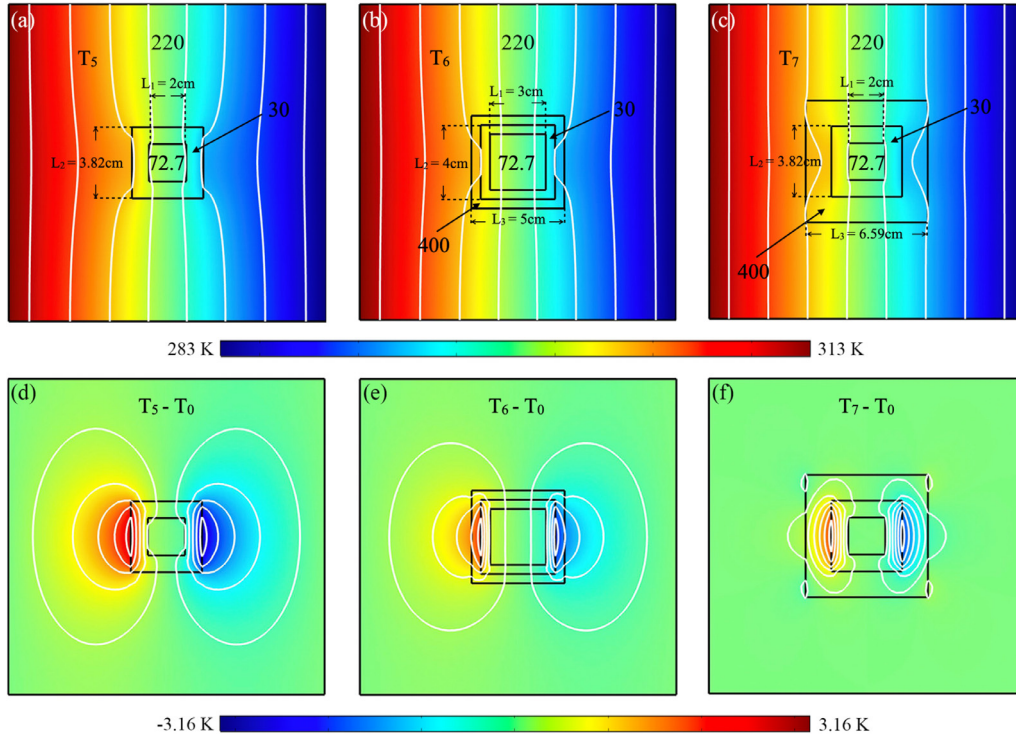
Fig. 5. Simulation results of square bilayer thermal sensors. The simulation box is 17×17 cm^2. White lines represent isotherms. Sensor, inner shell, outer shell, and background are respectively expanded Magnesium alloy, Stainless steel, Copper, and Aluminum with conductivity of 72.7, 30, 400, and 220 W m^{-1} K^{-1}. (a) Thermal sensor of single layer size with $L_1 = 2$ cm and $L_2 = 3.82$ cm. (b) Bilayer thermal sensor of random size with $L_1 = 3$ cm, $L_2 = 4$ cm and $L_3 = 5$ cm. (c) Bilayer thermal sensor of optimized size with $L_1 = 2$ cm, $L_2 = 3.82$ cm and $L_3 = 6.59$ cm. (d),(e),(f) Temperature difference between (a),(b),(c) and Fig. 3(a).

racy and invisibility are, respectively, defined as,

$$\Psi_s = \frac{1}{N_s} \sum_{i=1}^{N_s} \left| T(i) - T_{ref}(i) \right|, \tag{10}$$

$$\Psi_b = \frac{1}{N_b} \sum_{i=1}^{N_b} \left| T(i) - T_{ref}(i) \right|, \tag{11}$$

where i, T, T_{ref}, N_s, and N_b represent sequence number of nodes, temperature distribution controlled by bilayer thermal sensor, temperature distribution in pure background, number of nodes in sensor and background regions after discretization, respectively. Then

we add Eqs. (10) and (11) to represent the fitness function,

$$\Psi = \Psi_s + \Psi_b. \tag{12}$$

As a swarm intelligence optimization algorithm, PSA [Fig. 2] has a very high convergence rate, adopted extensively for inverse problems. PSA gets the optimal solution through the coordination of particles in the solution space, and particles constantly follow the current optimal particle. To solve the optimal problem mentioned above, we first initialize N particles R_j^0 j=1,2,...,N, in the feasible solution space K, given as

$$K = \left\{ R = (R_1, R_2, R_3) : R_{min} \leq R_i < R_j \leq R_{max}, \right.$$
$$\left. i < j; \ i, \ j \in \{1, 2, 3\} \right\}. \tag{13}$$
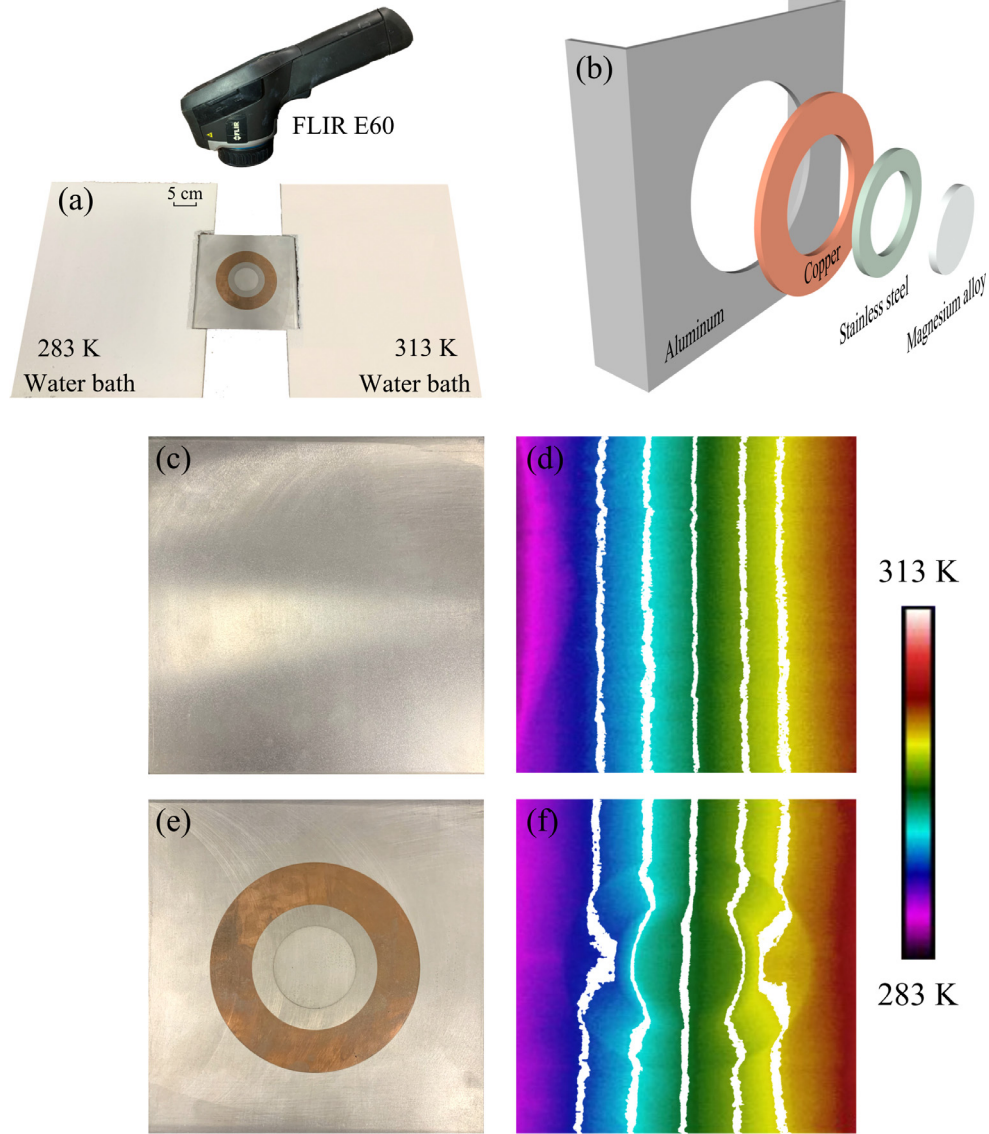
Fig. 6. Laboratory experiments. (a) Experimental setup. (b) Composition of bilayer thermal sensor. (c),(e) Real photos of reference and bilayer thermal sensor. (d),(f) Measured results for (c),(e). White lines represent isotherms. The sample size in (c) and (e) is the same as that for Fig. 3(a) and (g).

The characteristics of each particle are represented by position, velocity and fitness function in K space. Particles move constantly in the solution space, updating the position and velocity of individuals by tracking individual and group extremum points. Here, individual and group extremum points are the positions with the minimum fitness function among all the positions experienced by the individual and group particles. Each time positions of particles are updated, the fitness function of which are calculated. During each iteration, the updating formula of particlesvelocity and position are respectively as follows:

$$V_j^{i+1} = wV_j^i + c_1 d_1 \left(P_j^i - R_j^i \right) + c_2 d_2 \left(P_g - R_j^i \right), \quad (14)$$

$$R_j^{i+1} = R_j^i + V_j^{i+1}, \quad (15)$$

where i is iteration number, j is sequence number of each particle, P_j^i is individual extremum point of jth particle at the ith iteration, and P_g is group extremum point. w is inertia weight usually taken as a linear decreasing function, denoted by

$$w = w_s - (w_s - w_e) \frac{i}{I_{\max}}, \quad (16)$$

Table 1
Parameter setting of optimization model.

N	w_s	w_e	$I_{\max}$	c_1	c_2
50	0.9	0.4	150	1.49	1.49

where w_s, w_e, and $I_{\max}$ are respectively initial inertia weight (for global search), final inertia weight (for local search), and total number of iteration. c_1 and c_2 are empirical constant. d_1 and d_2 are random numbers between 0 and 1. Relevant parameters of the optimization model are shown in Table 1. When finishing total iterations, termination conditions are met (or say minimum fitness function converged). Therefore, we get the optimal solution for design variables. Also, we have finished the design of bilayer thermal sensors.

On the same footing, we extend bilayer thermal sensors to a square case, in which there is no strict analytical theory of bilayer thermal sensors. For a given set of four different bulk isotropic materials, the sides of three squares (L_1, L_2 and L_3, from inside to outside) are selected as design variables. Using PSA, we can obtain

the geometrical size of bilayer thermal sensor with the best performance of accuracy and invisibility.

4. Finite-element simulations

With each suitable set of selected materials, we obtain the optimal solution R of the design variables, which represent the radius of sensor, inner shell and outer shell. For numerical demonstrations, we choose two different materials for the inner shell (Inconel alloy 625 and Stainless steel 436 with conductivity of 9.8 and 30 W m^{-1} K^{-1}) to perform finite-element simulations with COMSOL MULTIPHYSICS. Sensor, outer shell and background are respectively expanded Magnesium alloy, Copper, and Aluminum with conductivity of 72.7, 400, and 220 W m^{-1} K^{-1}. Thus, we get two sets of design variables, parameterizing two cases of bilayer thermal sensors.

Before discussing the results of bilayer thermal sensors, we first show two reference schemes; one for pure background [Fig. 3(a)], the other for bare sensor [Fig. 3(b) and (f)]. Apparently, the presence of bare sensor disturbs thermal field of pure background, also making thermal field in sensor region distorted. Fig. 3(c) and (g) show the simulation results of two cases of bilayer thermal sensors designed by PSA. It is clear that external isotherms in two cases are both vertical. Also in two cases, the interval between internal isotherms (in sensor region) are almost the same as those in pure background. For accentuating the temperature difference, we plot the difference distributions between various schemes and pure background. From Fig. 3(d) and (h), we get a big temperature deviation in sensor and background regions imposed by bare sensors. On the contrary, temperature difference in sensor and background regions in Fig. 3(e) and (i) is almost zero. Furthermore, the temperature distributions along y axis on Line 1 in Fig. 3 are exported for contrasting the performance of these schemes quantitatively; see Fig. 4. Clearly, for each bilayer thermal sensor, it maintains the same temperature distributions in sensor and background regions as those in pure background, which demonstrates its excellent performance. However, bare sensor not only makes measurement in sensor region inaccurate, but also distorts thermal field in background region, whose temperature difference (TD) is shown in the upper right inset of Fig. 4.

Moreover, we also perform finite-element simulations of square bilayer thermal sensors with different geometrical size (structure with single shell, structure with bilayer shell of random size and structure with bilayer shell of optimized size). As expected, optimized size greatly improves the performance of thermal sensor, reproducing temperature distributions in sensor and background regions from original thermal field; see Fig. 5.

5. Laboratory experiments

To test the performance of the bilayer thermal sensor, we select one case [Fig. 3(g)] to conduct the experiment with a setup shown in Fig. 6(a). For comparison, we prepare two samples, one for background with pure Aluminum [Fig. 6(c)]; another for the bilayer scheme made of Magnesium alloy (AZ91D), Stainless steel (ASTM 436), Copper, and Aluminum (from inside to outside) [Fig. 6(e)]. Both of them have the size of $22 \times 22 \times 0.5$ cm^3, each with two tentacles 5 cm high on the left and right respectively. Sensor (R_1), inner shell (R_1 and R_2), and outer shell (R_2 and R_3) have the circular boundaries with the radii of $R_1 = 2.73$ cm, $R_2 = 4.11$ cm, and $R_3 = 6.85$ cm. We process the structure of four materials by laser cutting and combine these parts using mechanics enchases craft, as shown in Fig. 6(b). The left and right tentacles of samples are respectively immersed in 283 K and 313 K water bath, and an infrared camera FLIR E60 is used to measured the temperature distributions of two samples at steady state (after 10 min). Fig. 6(d) and

(f) show the measured results of Fig. 6(c) and (e), respectively. Obviously, though thermal contact resistance exists in the interface of different materials, our scheme exhibits excellent property in both accuracy and thermal invisibility, which is well consistent with the simulation result of Fig. 3(g).

6. Conclusion

In summary, we have proposed an optimization model with particle swarm algorithms for designing bilayer thermal sensors composed of bulk isotropic materials. As an example, we design and fabricate a circular bilayer thermal sensor with high performance, as both simulation result and experimental result exhibit. Such a scheme removes the need of extreme parameters (anisotropic, graded or singular), making engineering applications readily and efficiently. Optimization model can also be flexibly extended to a square case. Finally, an intelligent method of simplifying structures and materials can not only calculate numerical solutions for difficult analytical theories (circular structure), but also calculate optimal solutions for problems without analytical theories (square structure). This provides an insight into the development of metamaterials in a wide range of communities.

Declaration of Competing Interest

Authors declare that they have no conflict of interest.

CRediT authorship contribution statement

Peng Jin: Conceptualization, Formal analysis, Writing - original draft. **Shuai Yang:** Writing - original draft. **Liujun Xu:** Writing - original draft. **Gaole Dai:** Writing - original draft. **Jiping Huang:** Conceptualization, Writing - original draft. **Xiaoping Ouyang:** Writing - original draft.

Acknowledgments

References

[1] U. Leonhardt, Optical conformal mapping, Science 312 (2006) 1777–1780.
[2] J.B. Pendry, D. Schurig, D.R. Smith, Controlling electromagnetic fields, Science 312 (2006) 1780–1782.
[3] C.Z. Fan, Y. Gao, J.P. Huang, Shaped graded materials with an apparent negative thermal conductivity, Appl. Phys. Lett. 92 (2008) 251907.
[4] T.Y. Chen, C.N. Weng, J.S. Chen, Cloak for curvilinearly anisotropic media in conduction, Appl. Phys. Lett. 93 (2008) 114103.
[5] S. Narayana, Y. Sato, Heat flux manipulation with engineered thermal materials, Phys. Rev. Lett. 108 (2012) 214303.
[6] X. He, L.Z. Wu, Thermal transparency with the concept of neutral inclusion, Phys. Rev. E 88 (2013) 033201.
[7] C.J. Yu, Y.H. Li, X. Zhang, X. Huang, V. Malyarchuk, S.D. Wang, Y. Shi, L. Gao, Y.W. Su, Y.H. Zhang, H.X. Xu, R.T. Hanlon, Y.G. Huang, J.A. Rogers, Adaptive optoelectronic camouflage systems with designs inspired by cephalopod skins, Proc. Natl. Acad. Sci. USA 111 (2014) 12998.
[8] H.Y. Xu, X.H. Shi, F. Gao, H.D. Sun, B.L. Zhang, Ultrathin three-dimensional thermal cloak, Phys. Rev. Lett. 112 (2014) 054301.
[9] Y.G. Ma, Y.C. Liu, M. Raza, Y.D. Wang, S.L. He, Experimental demonstration of a multiphysics cloak: manipulating heat flux and electric current simultaneously, Phys. Rev. Lett. 113 (2014) 205501.
[10] T.C. Han, X. Bai, D.L. Gao, J.T.L. Thong, B.W. Li, C.W. Qiu, Experimental demonstration of a bilayer thermal cloak, Phys. Rev. Lett. 112 (2014) 054302.
[11] T.Z. Yang, X. Bai, D.L. Gao, L.Z. Wu, B.W. Li, J.T.L. Thong, C.W. Qiu, Invisible sensors: simultaneous sensing and camouflaging in multiphysical fields, Adv. Mater. 27 (2015) 7752.

[12] T.C. Han, P. Yang, Y. Li, D.Y. Lei, B.W. Li, K. Hippalgaonkar, C.W. Qiu, Full-parameter omnidirectional thermal metadevices of anisotropic geometry, Adv. Mater. 30 (2018) 1804019.

[13] R. Hu, S.L. Zhou, Y. Li, D.Y. Lei, X.B. Luo, C.W. Qiu, Illusion thermotics, Adv. Mater. 30 (2018) 1707237.

[14] R. Hu, S.Y. Huang, M. Wang, X.B. Luo, J. Shiomi, C.W. Qiu, Encrypted thermal printing with regionalization transformation, Adv. Mater. 31 (2019) 1807849.

[15] J. Shang, R.Z. Wang, C. Xin, G.L. Dai, J.P. Huang, Macroscopic networks of thermal conduction: failure tolerance and switching processes, Int. J. Heat Mass Transf. 121 (2018) 321.

[16] J. Qin, W. Luo, P. Yang, B. Wang, T. Deng, T.C. Han, Experimental demonstration of irregular thermal carpet cloaks with natural bulk material, Int. J. Heat Mass Transf. 141 (2019) 487.

[17] G.L. Dai, J.P. Huang, Nonlinear thermal conductivity of periodic composites, Int. J. Heat Mass Transf. 147 (2020) 118917.

[18] L.J. Xu, J.P. Huang, Controlling thermal waves with transformation complex thermotics, Int. J. Heat Mass Transf. 159 (2020) 120133.

[19] L.L. Zhou, S.Y. Huang, M. Wang, R. Hu, X.B. Luo, While rotating while cloaking, Phys. Lett. A 383 (2019) 759.

[20] R. Hu, S.Y. Huang, M. Wang, L.L. Zhou, X.Y. Peng, X.B. Luo, Binary thermal encoding by energy shielding and harvesting units, Phys. Rev. Appl. 10 (2018) 054032.

[21] L.J. Xu, S. Yang, J.P. Huang, Thermal transparency induced by periodic interparticle interaction, Phys. Rev. Appl. 11 (2019) 034056.

[22] J.X. Li, Y. Li, T.L. Li, W.Y. Wang, L.Q. Li, C.W. Qiu, Doublet thermal metadevice, Phys. Rev. Appl. 11 (2019) 044021.

[23] L.J. Xu, S. Yang, J.P. Huang, Passive metashells with adaptive thermal conductivities: chameleonlike behavior and its origin, Phys. Rev. Appl. 11 (2019) 054071.

[24] L.J. Xu, J.P. Huang, Metamaterials for manipulating thermal radiation: transparency, cloak, and expander, Phys. Rev. Appl. 12 (2019) 044048.

[25] B.I. Popa, S.A. Cummer, Cloaking with optimized homogeneous anisotropic layers, Phys. Rev. A 79 (2009) 023806.

[26] E.M. Dede, T. Nomura, J. Lee, Thermal-composite design optimization for heat flux shielding, focusing, and reversal, Struct. Multidiscip. Optim. 49 (2014) 59–68.

[27] E.M. Dede, P. Schmalenberg, T. Nomura, M. Ishigaki, Design of anisotropic thermal conductivity in multilayer printed circuit boards, IEEE Trans. Compon. Packag. Manuf. Technol. 5 (2015) 1763–1774.

[28] I. Peralta, V.D. Fachinotti, Optimization-based design of heat flux manipulation devices with emphasis on fabricability, Sci. Rep. 7 (2017) 6261.

[29] G. Fujii, Y. Akimoto, M. Takahashi, Exploring optimal topology of thermal cloaks by CMA-ES, Appl. Phys. Lett. 112 (2018) 061108.

[30] G. Fujii, Y. Akimoto, Optimizing the structural topology of bifunctional invisible cloak manipulating heat flux and direct current, Appl. Phys. Lett. 115 (2019) 174101.

[31] G.V. Alekseev, D.A. Tereshko, Particle swarm optimization-based algorithms for solving inverse problems of designing thermal cloaking and shielding devices, Int. J. Heat Mass Transf. 135 (2019) 1269–1277.

[32] G. Fujii, Y. Akimoto, Topology-optimized thermal carpet cloak expressed by an immersed-boundary level-set method via a covariance matrix adaptation evolution strategy, Int. J. Heat Mass Transf. 137 (2019) 1312.

[33] G. Fujii, Y. Akimoto, Cloaking a concentrator in thermal conduction via topology optimization, Int. J. Heat Mass Transf. 159 (2020) 120082.

[34] R. Hu, X.B. Luo, Two-dimensional phonon engineering triggers microscale thermal functionalities, Natl. Sci. Rev. 6 (2019) 1071.

[35] R. Hu, S. Iwamoto, L. Feng, S.H. Ju, S.Q. Hu, M. Ohnishi, N. Nagai, K. Hirakawa, J. Shiomi, Machine-learning-optimized aperiodic superlattice minimizes coherent phonon heat conduction, Phys. Rev. X 10 (2020) 021050.

[36] R. Hu, J.L. Song, Y.D. Liu, W. Xi, Y.T. Zhao, X.J. Yu, Q. Cheng, G.M. Tao, X.B. Luo, Machine learning-optimized Tamm emitter for high-performance thermophotovoltaic system with detailed balance analysis, Nano Energy 72 (2020) 104687.

[37] R. Poli, J. Kennedy, T. Blackwel, Particle swarm optimization: an overview, Swarm Intel. 1 (2007) 33–57.

[38] P. Jin, L.J. Xu, T. Jiang, L. Zhang, J.P. Huang, Making thermal sensors accurate and invisible with an anisotropic monolayer scheme, Int. J. Heat Mass Transf. 163 (2020) 120437.

[39] http://www.comsol.com/.